JOURNAL OF FORENSIC SCIENCES

J Forensic Sci, September 2011, Vol. 56, No. 5
doi: 10.1111/j.1556-4029.2011.01808.x
Available online at: onlinelibrary.wiley.com

TECHNICAL NOTE

CRIMINALISTICS

John W. Bond,[1,2] *D.Phil.*

Effect of Temperature on Rectifying Schottky Barriers Formed from Fingerprint Sweat Corrosion of Brass

ABSTRACT: Corrosive electrochemical processes of brass, including those resulting from fingerprint sweat, continue to be studied because of the widespread industrial use of brass. Here, we examine how increased temperature affects the relative abundance of fingerprint sweat corrosion products and the rectifying Schottky barrier formed between p-type copper (I) oxide corrosion and brass. X-ray photoelectron spectroscopy confirms increasing dezincification with increasing temperature. This leads to n-type zinc oxide replacing copper (I) oxide as the dominant corrosion product, which then forms a rectifying Schottky barrier with the brass, instead of copper oxide, when the temperature reaches *c.* 600°C. Using X-ray diffraction, resulting diodes show polycrystalline oxides embedded in amorphous oxidation products that have a lower relative abundance than the diode forming oxide. Conventional current/voltage (I/V) characteristics of these diodes show good rectifying qualities. At temperatures between *c.* 100 and *c.* 600°C, when neither oxide dominates, the semiconductor/brass contact displays an absence of rectification.

KEYWORDS: forensic science, latent fingerprint, print visualization, metal corrosion, electrochemical mechanism, Schottky barrier

Brass attracts widespread use in a range of industries because of its favorable thermal and mechanical properties, and, as a consequence, corrosive electrochemical processes of brass continue to be studied (1–5). Recent research has shown how fingerprint patterns deposited as sweat on brass shell casings can be visualized as a result of an electrochemical reaction between the sweat and brass (6–8). This reaction can lead to the formation of a rectifying Schottky barrier contact between p-type copper (I) oxide corrosion formed on the surface of the brass and the brass substrate (9). When this occurs, a positive potential (V) applied to the brass substrate has been shown to vary exponentially with that measured on an area of fingerprint sweat corrosion, with a potential difference ($\triangle$V) of up to *c.* 10V for $V = 1400$V (9). With $\triangle$V of this magnitude, a fine carbon powder (particle size *c.* 10 μm) introduced to the brass has been found to adhere preferentially to the areas of corrosion, thus enabling the fingerprint to be visualized (8). Such visualization has been achieved even after the sweat deposit has been removed from the brass (10). Thus, rectifying Schottky barrier formation and the application of a positive V to the brass substrate is thought to be indicative of yielding $\triangle$V of sufficient magnitude to enable fingerprint sweat corrosion to be visualized (11).

A rectifying Schottky barrier of this type (metal to p-type semiconductor) requires the work function of the metal (φ_{brass}) to be less than the work function of the semiconductor ($\varphi_{s\text{-}c}$) (12). The work function of a solid (φ) is defined as the minimum energy required to remove an electron from the Fermi-level energy of the solid (E_F) to the vacuum-level energy. Figure 1*a* shows a schematic representation of an energy-level diagram for a metal (metal "A") and a p-type semiconductor in which the work function of the metal (φ_{brass}) is less than the semiconductor ($\varphi_{s\text{-}c}$). As this is an energy-level diagram, work functions are shown as energies (multiplied by *q*, the electronic charge), rather than as potentials. As $\varphi_{brass} < \varphi_{s\text{-}c}$, the Fermi-level energy of the metal ($E_{F(brass)}$) is greater than the semiconductor ($E_{F(s\text{-}c)}$). For the semiconductor, the electron valence band (E_v) and conduction band (E_c) energy levels are also shown. In Fig. 1*b*, the metal and semiconductor have been brought into contact resulting in electron flow from the metal to the semiconductor as $\varphi_{brass} < \varphi_{s\text{-}c}$. Electron flow continues until the Fermi levels in both materials are aligned and $E_{F(brass)} = E_{F(s\text{-}c)}$. The electric field generated by this electron flow acts to oppose further movement of charge, a situation known as thermal equilibrium. This electron flow and Fermi-level alignment result in a bending of the semiconductor conduction and valence bands upward as shown and a depletion of the concentration of majority carrier holes in the vicinity of the metal–semiconductor junction. This majority carrier depletion extends a distance W into the semiconductor as shown in Fig. 1*b*. The net result is the creation of a potential barrier (φ_b) that must be overcome by the majority carrier holes for a conduction current to flow between the metal and semiconductor. A positive or negative bias potential applied to the semiconductor (with respect to the metal) has the effect of either lowering or raising the potential barrier, thereby giving rise to a practical application of a rectifying Schottky barrier, namely a Schottky barrier diode. Figure 1*c* shows a schematic representation of a Schottky barrier diode forward (or positive) biased in an electrical circuit and formed with a rectifying Schottky barrier between a metal (metal "A") and a p-type semiconductor. Electrical contact is made to the other end of the semiconductor with a metal (metal "B") that has a work function greater than the semiconductor,

[1]Northamptonshire Police, Force HQ, Wootton Hall, Northampton NN4 OJQ, U.K.
[2]Forensic Research Centre, University of Leicester, Leicester LE1 7EA, U.K.

Received 24 May 2010; and in revised form 7 Aug. 2010; accepted 22 Aug. 2010.

© 2011 American Academy of Forensic Sciences

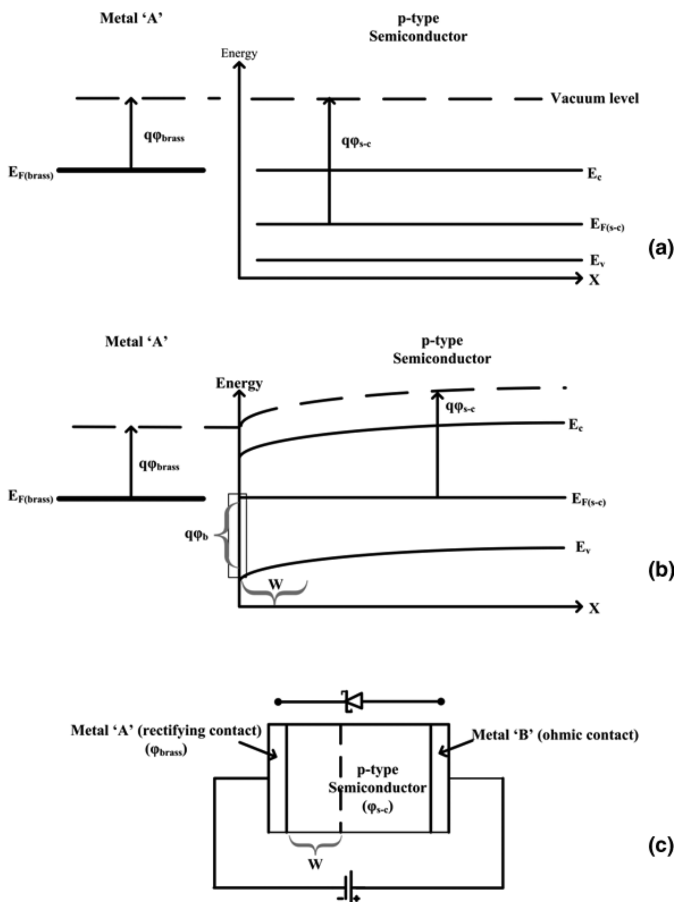

FIG. 1—*Schematic representation of the energy level diagram for a metal and p-type semiconductor in which the work function of the metal is less than the work function of the semiconductor. (a) shows the two materials separated and (b) in contact with a resulting bending of the semiconductor energy bands. W represents the width of the majority carrier depletion in the semiconductor and qΦb the energy of the potential barrier. (c) shows a schematic representation of a Schottky barrier diode formed from a metal and p-type semiconductor and forward biased.*

thereby giving rise to an ohmic contact rather than a rectifying contact.

An analogous situation may be described in which the semiconductor is n-type. In this case, a rectifying Schottky barrier is formed between the metal and n-type semiconductor when $\varphi_{\text{brass}} > \varphi_{\text{s-c}}$ with the semiconductor conduction and valence bands bending downward and a depletion of the concentration of majority carrier electrons in the vicinity of the metal–semiconductor junction. Clearly, the polarity of the applied bias potential necessary to lower the barrier potential (φ_b) is the opposite to that required for a metal to p-type semiconductor (12).

Lately, we have shown that when zinc oxide dominates the corrosion product, fingerprint sweat corrosion can be visualized using the carbon powder described previously, but with a negative (rather than a positive) V. We postulated that this might be as a result of the formation of an n-type zinc oxide/brass rectifying Schottky barrier contact (12,13).

Complementing research on saline (1,3–5) and elevated temperature corrosion of brass (14), in this technical note, we examine how increased temperature affects the relative abundance of fingerprint sweat corrosion products and rectifying contact formation. Such studies are of importance to those engaged in researching the recovery of fingerprints from brass shell casings (15) or arson crime scenes (16). Also, corrosion of brass by fingerprint sweat has relevance to the control of the surface properties of brass (17).

Materials and Methods

Forty donors each deposited fingerprint sweat onto 1-mm-thick 25-mm-diameter α-phase brass disks (68Cu-32Zn by percentage weight) such that each donor provided a deposit on five disks (9,11,18). The technique for measuring rectifying characteristics has been described previously (11) with, briefly, electrical contact being made with corroded areas of a disk by means of a platinum probe formed into a tip *c.* 55 μm diameter (9,11). Platinum was selected as it forms an ohmic contact with copper (I) oxide (9,11). Ten days after deposition, one disk from each donor was washed in a 0.5-L solution of warm water containing a few drops of commercial detergent and rubbed vigorously with a nonabrasive cloth. This washing regime has been shown to remove effectively the fingerprint deposit (but not the corrosion) from the surface of the brass disk (18). Conventional forward bias current/voltage (I/V) measurements were then taken for these disks and the goodness of fit of I/V to the diode equation (12).

$$I = AA^{**}T^2 \exp(-q\phi_B/kT)[\exp(qV/\eta kT) - 1]) \qquad (1)$$

assessed by means of a least squares regression analysis (19) for $0.4V \le V \le 0.55V$. In Eq. (1), A represents the electrically active contact area, A^{**} the effective Richardson constant, T the temperature, k is Boltzmann's constant, and η the ideality factor. The goodness of fit indicator (R^2) is defined as $0 \le R^2 \le 1$ with $R^2 = 1$ indicating a perfect fit between observed and estimated values (19). The range of V was selected to maximize R^2. An assessment of the goodness of fit of each disk to the diode equation was necessary to identify those disks where the metal/corrosion product interface displayed a rectifying Schottky barrier. Measuring the I/V characteristics of the metal/corrosion product has been used previously as a means of identifying the presence of a rectifying Schottky barrier (9).

Results and Discussion

Following these measurements, only disks giving a statistically significant R^2 ($p < 0.001$) were considered for further analysis. This left the five disks from just two of the 40 donors with the examined disk from each donor having $R^2 = 0.99$. Of these five disks from each donor, one was taken as an ambient temperature sample, referred to subsequently as A1 (donor 1) and A2 (donor 2). The remaining four disks from each donor were heated over a Bunsen flame to 100, 200, 400, or 600°C and then washed as described earlier (18). This temperature range encompassed that used by other workers examining the effect of heating brass or copper (14,17,20) and is also consistent with what might be encountered in an arson crime scene (16,21). These eight heated disks are referred to subsequently as B1, B2 (100°C), C1, C2 (200°C), D1, D2 (400°C), and E1, E2 (600°C). Figure 2 shows the fingerprint corrosion pattern obtained from heated samples B1–E1.

Conventional I/V characteristics of all 10 disks were then measured with the platinum probe. Only A1 and A2 showed a rectifying contact with the other eight (heated) disks displaying an absence of rectification. The platinum probe was then replaced with a zinc probe and the I/V measurements repeated on all 10 disks. Zinc was selected as it forms an ohmic contact with n-type zinc oxide (22). Only E1 and E2 gave I/V characteristics consistent

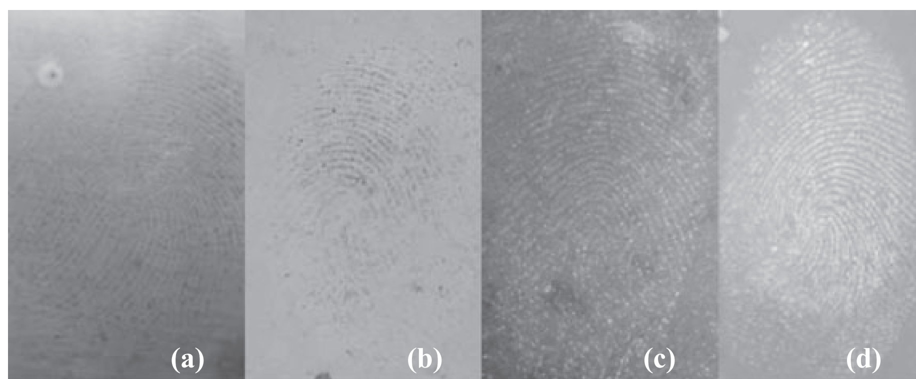

FIG. 2—*Disks (a) B1, (b) C1, (c) D1, and (d) E1 following heating to 100°C, 200°C, 400°C, and 600°C, respectively and washing.*

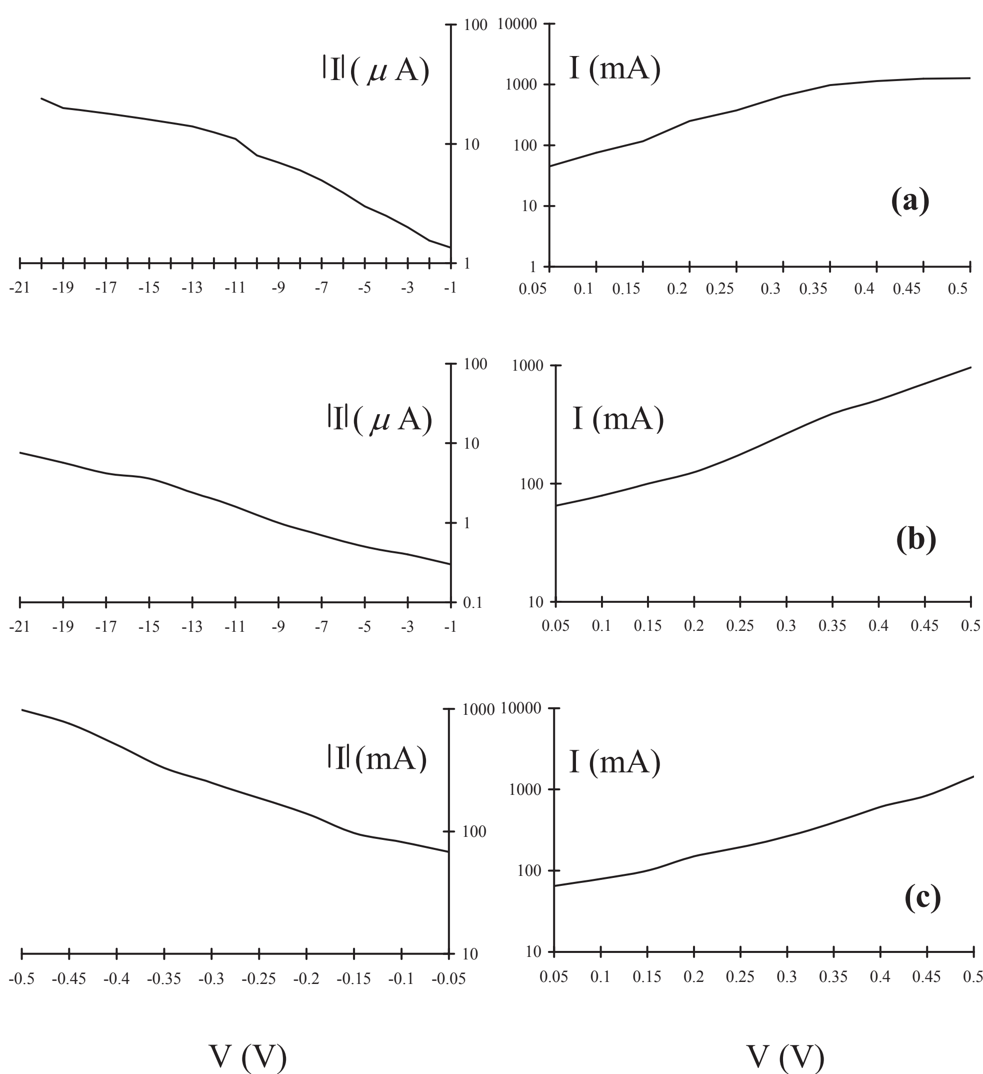

FIG. 3—*Conventional current/voltage plot for (a) A1 (ambient temperature) and platinum probe, (b) E1 (previously heated to 600°C) and zinc probe, and (c) B1 (previously heated to 100°C) and either zinc or platinum probe.*

with a rectifying contact, other disks displaying an absence of rectification. I/V plots for A1, B1, and E1 are shown in Fig. 3. B1 is included as a typical example of the absence of rectification, which has been observed widely for copper (I) oxide thin films deposited by electrochemical oxidation of the substrate (23–25). In Fig. 3, rectification is identified by the current (I) flowing across the barrier being orders of magnitude different for each polarity of V. This can be seen clearly for Fig. 3*a,b* where $V < 0$ gives a current of μA compared with $V > 0$, which gives a current of mA. For Fig. 3*c*, the current for both polarities of V is mA. This absence of

rectification has been ascribed to the formation of a thin insulating layer during the initial substrate–electrolyte interaction (23–25), the resulting diodes having I/V characteristics similar to metal-insulator-semiconductor tunnel diodes (12).

The surface corrosion of all 10 disks was examined by means of X-ray photoelectron spectroscopy (XPS), using a VG ESCALab 200d spectrometer (VG Scienta, Hastings, U.K.). Individual high-resolution spectra were taken at a pass energy of 50eV and an energy step of 0.05eV.

Figure 4 shows detailed Cu $2p_{3/2}$ spectra for A1–E1. The main peaks for A1 and B1 are characteristic of both metallic copper and copper (I) oxide (25,26). Cu(II) is characterized by a broader shake-up satellite *c.* 9eV higher than the Cu $2p_{3/2}$ peak (27,28), which is most evident for C1–E1.

The Cu $2p_{3/2}$ peaks were de-convoluted using standard Gaussian/Lorentzian functions (29), with the C1–E1 peaks indicating the presence of Cu(II). The Cu(II) component best matched copper (II) hydroxide for C1 and copper (II) oxide for D1 and E1.

A1–C1 gave an auger peak confirming the presence of copper (I) oxide (30), while A1–E1 gave an auger peak confirming the presence of zinc oxide (4). The Zn:Cu ratios for A1–E1 were 1:3.13, 1:1.92, 1:1.7, 1:1.36, and 1:0.78, respectively.

As disk temperature increased, so did both the oxidation state of copper and the surface concentration of zinc. The results for copper are consistent with previous results for heating α-phase brass (14) and copper (I) oxide thin films (20,27). Copper (II) hydroxide (C1) is likely formed during the initial electrochemical de-alloying with elevated temperatures for D1 and E1 dehydrating it to copper (II) oxide (31). XPS O1s spectra (not shown) showed a higher binding energy shoulder above the main O1s peak, which reduced as the disk temperature increased. This is consistent with surface hydroxide dehydrating to oxide (4).

An increase in the surface concentration of zinc above the bulk concentration during de-alloying is well documented (1,4) and is known as dezincification of brass, which is accelerated at elevated temperatures (14,32).

The crystalline quality of the oxide corrosion was then assessed by means of X-ray diffraction (XRD), using a Siemens D5000 diffractometer with a θ–2θ configuration (Bruker, Coventry, U.K.). XRD patterns with $10° \leq 2\theta \leq 70°$ and a 6° glancing angle (33,34) revealed that A1, A2, E1, and E2 exhibit a polycrystalline structure. Figure 5 shows the XRD pattern for A1 and E1.

A1 shows polycrystalline copper (I) oxide with a (111) preferred orientation ($2\theta = 36.6°$), as has been observed previously for electrodeposited copper (I) oxide films (23,35). E1 shows polycrystalline zinc oxide with a (002) preferred orientation ($2\theta = 34.4°$) and this has been observed previously for both electrodeposited zinc oxide films (35) and oxidation of α-phase brass (36). E1 also shows weak copper (II) oxide XRD peaks ($2\theta = 35°, 55.4°$), observed previously for copper (II) oxide thin films (33). The XRD spectrum for E1 confirms the presence of both copper (II) oxide and zinc oxide.

Depth profiling of A1, B1, and E1 was then undertaken by sputtering with an Ar^+ ion beam (1 KeV) in combination with XPS and Auger electron spectroscopy. The sputtering rate was 1 nm/min. Figure 6 shows the Cu/Zn ratio as a function of sputtering depth (d). A1 for $d < 50$ nm and B1 for $d < 55$ nm best matched copper (I) oxide and zinc oxide, while E1 for $d < 95$ nm best matched copper (II) oxide and zinc oxide. Above these values

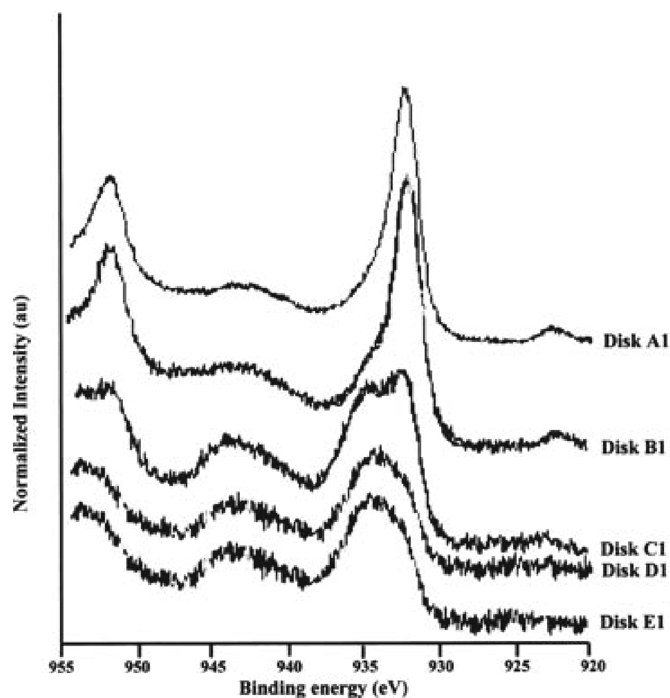

FIG. 4—*X-ray photoelectron spectroscopy detail spectra for A1–E1 showing the Cu 2p3/2 peak and higher binding energy shakeup satellite.*

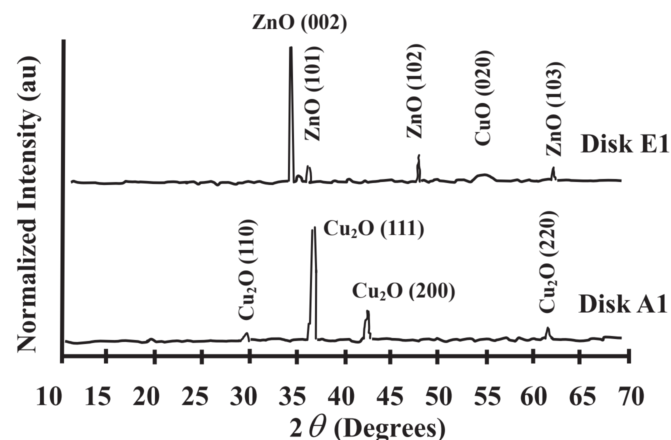

FIG. 5—*X-ray diffraction spectra for A1 and E1.*

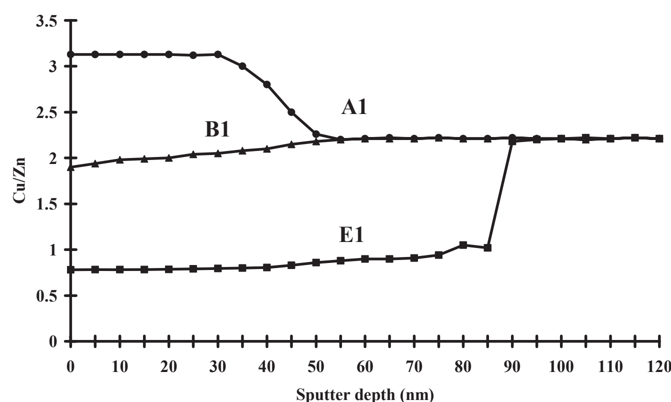

FIG. 6—*X-ray photoelectron spectroscopy depth profiles for A1, B1, and E1.*

of d, all three disks best matched metallic copper and zinc. Oxide films of this thickness are consistent with those reported for electrochemical de-alloying of α-phase brass in aqueous saline (4).

Figure 3 may now be explained with reference to the XPS, XRD, and depth profile data. We have shown previously that a rectifying contact occurs when copper (I) oxide is abundant and Zn:Cu = 1:>3 (9). Clearly, when zinc oxide is abundant (E1), a rectifying contact is also observed but with a zinc (rather than platinum) probe. Thus, a rectifying contact may form between zinc oxide or copper (I) oxide and brass (12), the relative surface abundance of each oxide determining whether a rectifying contact is formed. The work function of the probe determines whether a rectifying contact is observed experimentally.

When neither oxide dominates (B1–D1), there is an absence of rectification. The depth profile for B1 shows a lack of any insulating layer between the surface semiconductor and bulk metal that, as described previously, would account for this (23–25). Instead, we propose the relative abundance of copper (I) and zinc oxides as the reason for the absence of rectification. For E1, the occurrence of an insulating copper (II) oxide layer between the surface zinc oxide and bulk metal did not affect the rectifying I/V characteristics. The effect that an insulating layer has on I/V characteristics is determined by the metal–insulator barrier height (ϕ_{mi}) and the thickness of the insulating layer (t) (12), with little effect for $\phi_{mi} <$ *c.* 3eV and t < *c.* 3 nm (12). For E1, ϕ_{mi} *c.* 0.53eV (11) and $t < 5$ nm.

Conclusion

Through a comparison of elevated temperature fingerprint sweat corrosion of α-phase brass by 40 different individuals, we have demonstrated that the oxidation state of copper and surface concentration of zinc both increase with increased temperature. Surface concentrations of zinc greater than those expected for un-corroded brass (Zn:Cu = 1:<2.2) are indicative of dezincification of the brass (32). With sufficient dezincification, n-type zinc oxide replaces p-type copper (I) oxide as the dominant corrosion product and this leads to the formation of a zinc oxide/brass rectifying Schottky barrier contact. Such a contact would be expected to enable fingerprint visualization provided a negative potential was applied to the brass as the polarity of a zinc oxide/brass diode is opposite to that of a copper (I) oxide/brass diode (because of zinc oxide and copper [I] oxide having different conductivity types [12]). When neither oxide dominates, there is a "mixed" zinc and copper corrosion product and an absence of rectification. In this case, any adherence of carbon powder to the areas of corrosion is likely to arise from the topography of the corrosion product. In addition to visualizing fingerprint sweat corrosion when copper (I) or zinc oxide corrosion dominates the surface of brass, rectifying Schottky barrier formation might also be used as a novel means of monitoring the relative abundance of brass corrosion products.

Acknowledgments

The author is indebted to the many members of Northamptonshire Police who, over an extended period, donated willingly their latent fingerprints for this research. The assistance of Mrs. Trudy Loe (Research Officer Northamptonshire Police) with the preparation of the manuscript is acknowledged with thanks.

The support of the Chief Officers of Northamptonshire Police in enabling this research to have been conducted is gratefully acknowledged.

References

1. Ateya BG, Al Kharafi AM, Ghayad IM. Dezincification of brass in hot, concentrated salt water. Corrosion 2009;65:419–26.
2. Alfantazi AM, Ahmed TM, Tromans D. Corrosion behaviour of copper alloys in chloride media. Mater Des 2009;30:2425–30.
3. Milosev I, Kosec T. Electrochemical and spectroscopic study of benzotriazole films formed on copper, copper-zinc alloys and zinc in chloride solution. Chem Biochem Eng Q 2009;23:53–60.
4. Kosec T, Merl DK, Milosev I. Impedance and XPS study of benzotriazole films formed on copper, copper-zinc alloys and zinc in chloride solution. Corrosion Sci 2008;50:1987–97.
5. Kosec T, Milosev I, Pihlar B. Benzotriazole as an inhibitor of brass corrosion in chloride solution. Appl Surf Sci 2007;253:8863–73.
6. Williams G, McMurray HN, Worsley DA. Latent fingerprint detection using a scanning Kelvin microprobe. J Forensic Sci 2001;46:1085–92.
7. Williams G, McMurray N. Latent fingermark visualization using a scanning Kelvin probe. Forensic Sci Int 2007;167:102–9.
8. Bond JW. Visualization of latent fingerprint corrosion of metallic surfaces. J Forensic Sci 2008;53:812–22.
9. Bond JW. Determination of the characteristics of a Schottky barrier formed by latent finger mark corrosion of brass. J Phys D Appl Phys 2009;42:235301.
10. Bond JW. Imaging fingerprint corrosion on fired brass shell casings. Rev Sci Instrum 2009;80:075108.
11. Bond JW. On the electrical characteristics of latent finger mark corrosion of brass. J Phys D Appl Phys 2008;41:125502.
12. Sze SM, Ng KK. Physics of semiconductor devices. Danvers, MA: Wiley, 2007.
13. Bond JW. Effect that the relative abundance of copper oxide and zinc oxide corrosion has on the visualization of fingerprints formed from fingerprint sweat corrosion of brass. J Forensic Sci 2011 April 6 [Epub ahead of print].
14. Beucher E, Lefez B, Lenglet M. Optical determination of cuprous oxide at zinc oxide-metal interface of an oxidized α brass. Phys Stat Sol (a) 1993;136:139–44.
15. Bond JW, Heidel C. Visualization of latent fingerprint corrosion on a discharged brass shell casing. J Forensic Sci 2009;54:892–4.
16. Deans J. Recovery of fingerprints from fire scene and associated evidence. Sci Justice 2006;46:153–68.
17. Wiame F, Salgin B, Swiatowska-Mrowiecka J, Maurice V, Marcus P. Brass surface nanochemistry: the role of alloying Cu with Zn. J Phys Chem C 2008;112:7540–3.
18. Paterson E, Bond JW, Hillman AR. A comparison of cleaning regimes for the effective removal of fingerprint deposits from brass. J Forensic Sci 2010;55:221–4.
19. Field A. Discovering statistics using SPSS. London, U.K.: Sage, 2008.
20. Papadimitropoulos G, Vourdas N, Em Vamvakas V, Davazoglou D. Deposition and characterization of copper oxide thin films. J Phys Conf Ser 2005;10:182–5.
21. DeHaan JD. Kirk's fire investigation, 4th rev. edn. Englewood Cliffs, NJ: Prentice Hall, 1997.
22. Kaye GWC, Laby TH. Tables of physical and chemical constants, 16th edn. Harlow, Essex, U.K.: Longman, 1995.
23. Mukhopadhyay AK, Chakraborty AK, Chatterjee AP, Lahiri SK. Galvanostatic deposition and electrical characterization of cuprous oxide thin films. Thin Solid Films 1992;209:92–6.
24. Ikata ES, Adjepong SK. Electrical characteristics of Cu-Cu_2O diodes fabricated by anodic oxidation. J Phys D Appl Phys 1988;21:1516–8.
25. Chatterjee AP, Mukhopadhyhay AK, Chakraboty AK, Sasmal RN, Lahiri SK. Electrodeposition and characterization of cuprous oxide films. Mater Lett 1991;11:358–62.
26. Tobin JP, Hirschwald W, Cunningham J. XPS and XAES studies of transient enhancement of CU-1 at CuO surfaces during vacuum outgassing. Appl Surf Sci 1983;16:411–4.
27. Al-Kuhaili MF. Characterization of copper oxide thin films deposited by the thermal evaporation of cuprous oxide (Cu_2O). Vacuum 2008; 82:623–9.
28. Kim KS. Charge-transfer transition accompanying X-ray photoionization in transition-metal compounds. J Electron Spectrosc 1974;3:217–26.
29. Shirley DA. Valence band structure from high resolution X-ray photoelectron spectroscopy (XPS). Phys Rev 1972;55:4709–14.
30. Ghodselahi T, Vesaghi MA, Shafiekhani A, Baghizadeh A, Lameii M. XPS study of the Cu@Cu_2O core shell nanoparticles. Appl Surf Sci 2008;255:2730–4.
31. Housecroft CE, Sharpe AG. Inorganic chemistry. Harlow, Essex, U.K.: Pearson, 2005.

32. Tretheway K, Chamberlain J. Corrosion for science and engineering. Harlow, Essex, U.K.: Addison Wesley Longman, 1998.
33. Gan ZH, Yu GQ, Tay BK, Tan CM, Zhao ZW, Fu Y. Preparation and characterization of copper oxide thin films deposited by filtered cathodic vacuum arc. J Phys D Appl Phys 2004;37:81–5.
34. Gumus C, Ozkendir OM, Kavak H, Ufuktepe Y. Structural and optical properties of zinc oxide thin films prepared by spraying pyrolysis method. J Optoelectron Adv M 2006;8:299–303.
35. Ikazi M, Shinagawa T, Mizuno K, Ida Y, Inaba M, Tasaka A. Electrochemically constructed p-Cu_2On-ZnO heterojunction diode for photovoltaic device. J Phys D Appl Phys 2007;40:3326–9.
36. Chang-Gyu P, Jung-Gu K, Yun Mo C, Jeon-Geon H, Seung-Ho A, Chang-Hee L. A study on corrosion characterization of plasma oxidized 65/35 brass with various frequencies. Surf Coat Technol 2005;200:77–82.

Additional information and reprint requests:
John W. Bond, D.Phil.
Scientific Support Department
Northamptonshire Police
Wootton Hall
Northampton NN4 OJQ
U.K.
E-mail: john.bond@northants.police.uk